



ISLAMIC UNIVERSITY OF TECHNOLOGY

**TITLE: NUMERICAL ANALYSIS OF A HIGHLY
SENSITIVE SOI MRR REFRACTIVE INDEX
SENSOR WITH PERFORMANCE
ENHANCEMENT USING GRAPHENE AND
GOLD**

By

Ahmed Shadman Alam (180021115)

Tasin Intisar (180021314)

Ishtiaqul Hoque (180021333)

This Thesis is Submitted in Consideration of Partial Fulfillment for the
Requirements of the Degree of BACHELOR OF SCIENCE IN ELECTRICAL AND
ELECTRONIC ENGINEERING

Department of Electrical and Electronic Engineering

Islamic University of Technology (IUT)

Board Bazar, Gazipur-1704, Bangladesh.

Academic Term: 2021-2022

Submitted on June 2023

DECLARATION

We, the authors of this report entitled " Numerical Analysis of a Highly Sensitive SOI MRR Refractive Index Sensor with Performance Enhancement Using Graphene and Gold ", hereby declare that this report and all the findings presented in it are our own.

Submitted by:

Shadman
5/6/23

Ahmed Shadman Alam
Student ID: 180021115

Tasin
05/06/23

Tasin Intisar
Student ID: 180021314

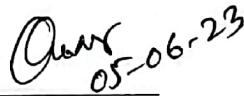
Ishtiaqul Hoque
05/06/23

Ishtiaqul Hoque
Student ID: 180021333

Certificate of Approval

The submitted report of our project entitled, “Numerical Analysis of a Highly Sensitive SOI MRR Refractive Index Sensor with Performance Enhancement Using Graphene and Gold” submitted by Ahmed Shadman Alam, St. No. 180021115, Tasin Intisar, St. No. 180021314, Ishtiaqul Hoque, St. No. 180021333 of Academic Year 2018-19 has been approved in June 2023.

Approved by:


05-06-23

Mr. Omar Faruque (Supervisor)

Associate Professor,

Electrical and Electronic Engineering Department,
Islamic University of Technology (IUT), Gazipur.

Acknowledgment

"All praise and gratitude be to Allah, the most beneficent, the most merciful."

We can never deny the endless mercy bestowed upon us by the Almighty Allah (SWT). At the very beginning, therefore, we express our deepest gratitude to the Almighty for granting us the wisdom and capability to reach this far with successful completion of this work. Alhamdulillah for everything!

We are grateful to our supervisor Mr. Omar Faruque, Associate Professor, Department of Electrical and Electronic Engineering, Islamic University of Technology (IUT), for his constant support throughout the whole year. His guidance, constant assistance, and knowledge has always inspired us to attain the best possible work. We appreciate him for making us realize the importance of self-learning.

To conclude we would like to mention our parents as it was never possible to achieve our goals without their mental support.

Table of Contents

Declaration.	ii
Certificate of Approval.	iii
Acknowledgement.	iv
Table Contents.	v
List of Figures.	vii
List of Tables.	ix
List of Abbreviations.	x
CHAPTER 1. Introduction	1
1.1 Background.	1
1.1.1 Photonics and Plasmonic.	3
1.1.2 Surface Plasmon Polaritons (SPPs).	3
1.1.3 Silicon-On-Insulator (SOI).	4
1.1.4 Micro Ring Resonators (MRR).	6
1.1.5 Graphene for Performance Enhancement.	9
1.1.6 Gold for Performance Enhancement.	10
1.1.7 Finite-Difference-Time-Domain (FDTD).	11
1.2 Literature Review.	15
1.3 Thesis Objective.	16
CHAPTER 2. Mechanism of Resonance in Mirroring Resonators And Parameters Analyzed.	18
2.1 Mechanism of Resonance in Micro Ring Resonators.	18
2.2 Sensitivity.	19
2.3 Figure of Merit (FOM).	21
CHAPTER 3. Main Work.	23
3.1 Recreating and Analyzing Past Models.	23
3.2 Basis of Optimization.	25

3.3 Optimization of Geometric Dimensions of MRR.	25
3.3.1 Optimization of the Rectangular Waveguide Width (W_1)	26
3.3.2 Optimization of the Resonator Height (H)	27
3.3.3 Optimization of the Coupling Gap (G)	28
3.3.4 Optimization of the Ring Width (W_2)	29
3.3.5 Optimization of the Ring Radius (R).	30
3.3.6 Optimized Simple Ring Resonator.	31
3.4 Scope of Improvement.	32
3.4.1 Depositing Graphene Layer.	32
3.4.2 Adding Gold Nano-disk.	32
CHAPTER 4. Results and Discussion.	34
4.1 Results.	34
4.2 Performance enhancement after addition of Gold and Graphene.	35
CHAPTER 5. Conclusion	36
5.1 Conclusion.	36
5.2 Future Work.	36
References	38

List of Figures

Figure 1a: Propagation of SPP	4
Figure 1b: Decay of SPP with time	4
Figure 1.2: Silicon-On-Insulator Structure	5
Figure 1.3: Micro Ring Resonator.	7
Figure 1.4: Graphene	10
Figure 1.5: Yee's Spatial Grid.	13
Figure 1.6: Yee's grid in 2D plane	14
Figure 1.7: Yee's grid in one dimension.	14
Figure 3.1: Generalized Parameters of SOI MRR.	24
Figure 3.2: Unoptimized SOI MRR Simulation.	25
Figure 3.3:	27
Figure 3.4.	28
Figure 3.5:	29
Figure 3.6:	30
Figure 3.7:	31
Figure 3.8: Optimized SOI MRR Simulation.	31
Figure 3.9: Optimized SOI MRR with Graphene Simulation.	32
Figure 3.10: Optimized SOI MRR with Gold Simulation.	33

List of Table

Table 3.1: Geometric parameters of unoptimized MRR.	24
Table 4.2: Optimized Geometric Parameters.	34
Table 4.3: Comparison of sensitivities with previous publications.	35

List of Abbreviations

SOI	Silicon-on-Insulator
MRR	Micro Ring Resonator
SPP	Surface Plasmon Polaritons
FDTD	Finite-Difference Time-Domain
FOM	Figure of Merit
RIU	Refractive Index Unit
FWHM	Full Width Half Maxima

Abstract

This study presents an innovative approach to designing an SOI ring resonator with enhanced sensing capabilities. Through meticulous optimization, we achieved an impressive figure of merit (FOM) of 56.15, indicating the remarkable efficiency of the device. Moreover, by incorporating a graphene layer atop the SiO₂ substrate, we effectively improved the interaction of light with the material, resulting in a notable sensitivity of 730 nm/RIU. To further enhance the sensor properties, we employed a plasmonic effect strategy by strategically placing a gold nano disk at the center of the ring structure on the graphene layer. Utilizing the FDTD method, we conducted comprehensive simulations to evaluate the performance of the proposed device in terms of sensitivity and FOM. The outstanding sensitivity of the device to changes in refractive index, as demonstrated by the simulation results, makes it a compelling choice for a wide range of sensing applications. The proposed design not only serves as a valuable blueprint for device fabrication but also paves the way for its practical implementation in real-world scenarios.

CHAPTER 1

INTRODUCTION

1.1 Background

Photonics is a fascinating field that revolves around the generation, manipulation, and detection of light. It encompasses various technologies and applications, including the development of optical devices and systems for communication, sensing, and imaging [1]. To design and analyze photonic devices, the Finite-Difference Time-Domain (FDTD) method is widely employed [2]. This numerical simulation technique accurately predicts how electromagnetic waves interact with complex structures, enabling the optimization of device performance. Micro-Ring Resonators (MRRs) are a prominent class of photonic devices that utilize circular waveguides to circulate light and form resonant modes, offering applications in sensing [3], filtering [4], and modulation [4]. Plasmonic, on the other hand, focuses on the interaction between light and metal nanoparticles by harnessing surface plasmons, enabling nanoscale light manipulation and enhanced device performance [5]. Within this section, we delve deeper into the principles and applications of Silicon-On-Insulator technology (SOI), MRRs, plasmonic, and the FDTD method, exploring their potential impact on advancing the field of photonics.

The advancement of silicon-based optical devices and integrated photonics led to the creation of SOI MRRs. In the late 1980s and early 1990s, a new area of study known as silicon photonics was born out of the need to use complementary metal-oxide semiconductor (CMOS) technology, which was already well-developed and well-established, for optical communication and sensing applications.

In the early stages, SOI-based waveguides, and passive components, such as couplers [6] and splitters, were the primary focus. However, researchers soon recognized the potential of micro ring resonators as highly sensitive and compact devices for various applications. The concept of MRRs originated from the field of microcavity photonics and resonant structures.

Micro ring resonators consist of a waveguide in the form of a ring, typically with a circumference on the order of micrometers. The resonator operates based on the principle of resonance, where the circulating light waves experience constructive interference at specific wavelengths. By controlling the dimensions and properties of the resonator, researchers could manipulate the resonant wavelengths and tailor the sensitivity and performance of the device [7].

The development of SOI MRRs gained momentum in the early 2000s, fueled by advances in fabrication techniques and the growing interest in silicon photonics for on-chip integration. Achieving tiny and high-performance devices required precise control over the dimensions and forms of the waveguides and resonators, which was made possible by fabrication techniques including reactive ion etching and electron beam lithography.

Researchers explored various design strategies to optimize the performance of SOI MRRs. By modifying parameters such as the ring radius, waveguide width, and coupling schemes, they could enhance the sensitivity, quality factor (Q-factor), and resolution of the resonators. Additionally, surface passivation techniques were developed to reduce optical losses and improve the overall performance of the devices [7].

SOI MRRs quickly found applications in sensing and detection. The label-free detection of biomolecules became a significant area of research, leveraging the interaction between the analyte and the evanescent field of the resonator. Biosensing applications[3], such as DNA detection [8], protein sensing[9], and label-free biosensors[8], demonstrated the potential of SOI MRRs for highly sensitive and selective detection platforms.

Looking ahead, the continued advancements in fabrication techniques, design strategies, and integration schemes are expected to drive further progress in SOI MRR technology. Ongoing research aims to address challenges such as reducing fabrication costs, enhancing temperature stability, and increasing the miniaturization and multiplexing capabilities of the devices[10].

In summary, the history of SOI MRRs can be traced back to the emergence of silicon photonics and the quest for leveraging CMOS technology for integrated optical devices. The development and refinement of SOI MRRs have led to their application in sensing and detection, offering high sensitivity, compactness, and compatibility with on-chip integration. With ongoing research, SOI

MRRs is poised to play a significant role in various areas, including biosensing, environmental monitoring, and optical communications.

1.1.1 Photonics and Plasmonic

The development of very sensitive optical sensors is greatly influenced by the fields of photonics and plasmonic. Designing and improving sensor devices may be done based on photonics, which places an emphasis on the creation, manipulation, and detection of light. The incorporation of plasmonic with photonics enables improved light-matter interactions at the nanoscale, providing chances to raise the sensitivity and effectiveness of the sensors. My study intends to develop the design and construction of a highly sensitive sensor based on an SOI ring resonator, graphene integration, and plasmonic effects to allow higher performance in a multitude of sensing applications by taking use of these complementary areas[11].

1.1.2 Surface Plasmon Polaritons (SPPs)

Surface plasmon polaritons (SPPs) are electromagnetic waves that differ from regular electromagnetic waves by as they migrate along the interface between a metal and a dielectric medium. In a micro-ring resonator (MRR), SPPs propagate through the metal-dielectric interface but are constrained to the subwavelength scale, allowing the electromagnetic field to localize close to the interface [12].

SPPs are distinguished by their exponential decay along the metal-dielectric interface. This decay is a result of energy loss due to Joule heating in the metal and electromagnetic field leakage into the dielectric medium encircling the metal. The decay length of SPPs, also known as the penetration depth, is dependent on the properties of the metal and dielectric materials as well as the incident light's wavelength [13].

Due to exponential decay, the propagation distance of SPPs is typically limited to a few micrometers or less, placing them near the metal-dielectric interface. This confinement facilitates strong light-matter interactions and allows for the nanoscale manipulation of light[14].

The exponential decay of SPPs along the metal-dielectric interface is essential for boosting the sensitivity of plasmonic sensors based on MRRs. Variations in the refractive index of the ambient medium influence the propagation and decay characteristics of the SPP when the MRR is subjected to these variations. Consequently, even minute variations in the refractive index can be detected via modifications in the transmission or resonance properties of the MRR[15].

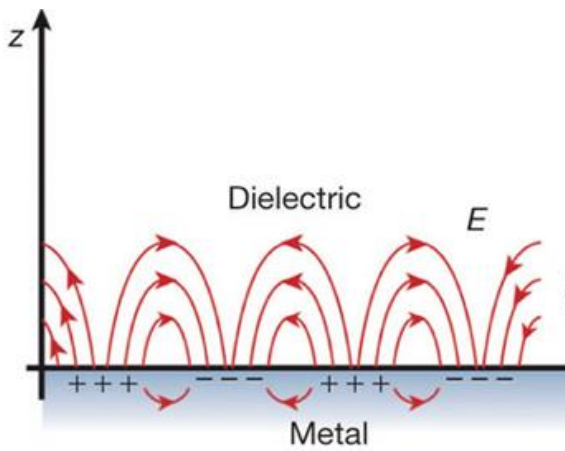


Figure 1a: Propagation of SPP

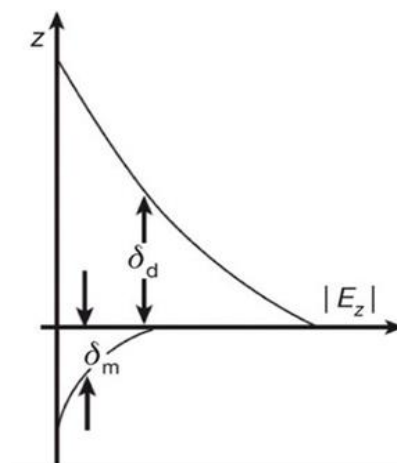


Figure 1b: Decay of SPP with time

1.1.3 Silicon-On-Insulator (SOI)

The creation of a thin layer of silicon on top of an insulating substrate, commonly silicon dioxide (SiO₂), is the process used in the semiconductor technology known as silicon-on-insulator (SOI). Comparing this approach to conventional bulk silicon wafers reveals several benefits.

The lower parasitic capacitance of SOI is a substantial benefit. The electrical capacitance between various components or transistors is reduced by adding an insulating layer between the active silicon layer and the substrate. As a result, the performance of the device is enhanced,

including switching speeds that are quicker, power consumption that is lower, and noise immunity that is better [16].

Better device isolation is another benefit of SOI. The insulating layer minimizes crosstalk and enhances circuit performance by preventing undesired electrical interactions between nearby components. This is especially helpful for highly integrated circuits where component density and miniaturization are crucial [17].

Lower power usage is another perk of SOI. The insulating layer serves as a barrier, decreasing power loss and enhancing the devices' energy efficiency. Because of this, SOI technology is especially well suited for low-power applications like those found in mobile and Internet of Things (IoT) devices[18].

Additionally, conventional complementary metal-oxide semiconductor (CMOS) processing is compatible with SOI technology. This means that SOI-based devices may be easily manufactured using current manufacturing methods and techniques utilized in the semiconductor industry, enabling the integration of SOI technology into current production lines simpler and more efficient[19].

All things considered, SOI technology has a few benefits, including a decrease in parasitic capacitance, enhanced device isolation, decreased power consumption, and compatibility with CMOS processing. Because of these advantages, SOI is a popular choice in many industries, including microelectronics, photonics, and integrated circuits. This has made it possible to create high-performance devices with increased functionality and efficiency.

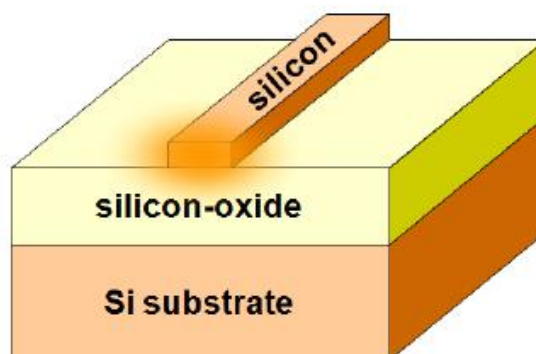


Figure 1.2: Silicon-On-Insulator Structure

1.1.4 Micro Ring Resonator (MRR)

Compact optical devices known as micro ring resonators (MRRs) take use of the phenomena of resonant light propagation in a circular waveguide construction. MRRs enable light to cycle several times within the ring, which results in resonant wavelengths and better optical qualities. MRRs consist of a ring-shaped waveguide with a tiny gap in the center of the waveguide. These minute structures have a variety of applications, including in the domains of sensing and optical signal processing, as well as in the field of telecommunications. MRRs often have several ports, such as through ports, input ports, and drop ports. Through the usage of the resonators through port, light may be passed through the device without having a substantial impact on its operation. The input port makes it possible to inject light into the ring, where it is subjected to several interactions that take place in a circular fashion within the resonator. A portion of the light that is being circulated can, under certain resonance conditions, be coupled out through the drop port. This results in the production of an output signal that can be selectively extracted at a certain resonant wavelength. MRRs are significant components in a variety of photonic applications due to the drop port capability that offers wavelength filtering and demultiplexing capabilities. These features make MRRs useful in optical communication systems, sensing devices, and on-chip signal processing, among other uses. MRRs are particularly desirable for obtaining efficient and integrated photonic functions because of their small size, high quality factors, and compatibility with technologies based on silicon. This opens the door for breakthroughs in a variety of sectors of optical research and technology.

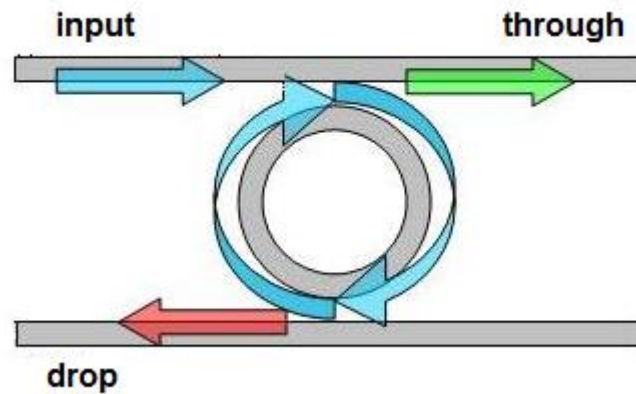


Figure 1.3: Micro Ring Resonator

Micro-ring resonators, often known as MRRs, are instruments that are utilized in optical sensing applications[1]. These MRRs are manufactured on silicon-on-insulator (SOI), which makes them incredibly sensitive. SOI MRRs takes advantage of the resonant behavior of light within a circular waveguide that has been created on an SOI substrate [20] to achieve the capability of wavelength-selective filtering or sensing. The SOI MRR is a type of waveguide-based optical resonator[21], and it is composed of a silicon waveguide that has a closed loop and a short radius. Typically, the radius is measured in the micrometer range. Since SiO₂ and Si have very different refractive indices, this substance is capable of functioning as a highly limited optical waveguide[22]. Because of the unique geometry of the ring resonator, it is possible to confine and recirculate light waves, which results in the production of resonant modes that have certain wavelengths or frequencies[20].

The fundamental operating principle of the MRR is based on whispering gallery mode (WGM)[23]. In sensors based on WGM optical resonators, light propagates as WGM resonances. These resonances are the result of light's total internal reflection along the curved surfaces of the resonator[24]. The WGM pattern generates a strong evanescent field at the interface between the waveguide and the ambient medium, with the strongest field occurring at the ring's equator. This field permeates the surrounding medium and interacts with any analyte molecules or particles that may be present. The interaction alters the effective index of refraction

n_{eff} of the optical WGM resonance. As a result, the cavity WGM resonance wavelength $\Delta \lambda_{WGM}$ experiences a net spectral shift. The well-established resonance condition links $\Delta \lambda_{WGM}$ and Δn_{eff} using the relationship [25]–[27]:

$$\Delta \lambda_{WGM} = \frac{2\pi R}{m} \Delta n_{eff} \quad (1.1)$$

where R stands for the ring radius, m for the integer mode order, and $\Delta \lambda_{WGM}$ stands for the wavelength [25]. Equation (1) only asserts that the resonance condition is met when an integer number of wavelengths is equal to the length of the round trip around the cavity [23]. The measurement of $\Delta \lambda_{WGM}$, which Δn_{eff} causes, makes it feasible to detect analytes. So, to proceed, we must first be able to determine the precise value for Δn_{eff} that the WGM resonance wavelength experiences in both the air and biological claddings [25]. The transmission spectrum of the input waveguide is used to track the resonances of WGM cavities [23]. where R stands for the ring radius, m for the integer mode order, and $\Delta \lambda_{WGM}$ stands for the wavelength [17]. Equation (1.1) only asserts that the resonance condition is met when an integer number of wavelengths is equal to the length of the round trip around the cavity [20]. The measurement of $\Delta \lambda_{WGM}$, which Δn_{eff} causes, makes it feasible to detect analytes. So, to proceed, we must first be able to determine the precise value for Δn_{eff} that the WGM resonance wavelength experiences in both the air and biological claddings [17]. The transmission spectrum of the input waveguide is used to track the resonances of WGM cavities [20].

The coupling between the ring resonator and the excitation signal (E_{i1}) provided at the input port are related by [24], [28], [29]:

$$\begin{pmatrix} E_{t1} \\ E_{t2} \end{pmatrix} = \begin{pmatrix} t & k \\ -k^* & t^* \end{pmatrix} \begin{pmatrix} E_{t1} \\ E_{t2} \end{pmatrix} \quad (1.2)$$

E_{t1} and E_{t2} are the normalized amplitudes of complex modes. The couplers' transmission coefficient (t) and coupling coefficient (k), which rely on one another based on [24]:

$$|t|^2 + |k|^2 = 1. \quad (1.3)$$

The following expression how waves propagate inside the ring segment of the resonator:

$$E_{i2} = E_{t2} L e^{-j\phi} \quad (1.4)$$

where ϕ is the accumulated phase and L is the loss coefficient for the propagation around the ring. The expression for the transmission coefficient and its phase is;

$$t = |t|e^{-j\phi_t}. \quad (1.5)$$

The transmitted field expression from equations (1.2), (1.3), (1.4), and (1.5) is expressed as,

$$E_{t1} = \frac{|t| - Le^{-j(\phi - \phi_t)}}{1 - |t|Le^{-j(\phi - \phi_t)}} E_{i1} e^{j\phi_t}. \quad (1.6)$$

The transmission loss $|t|$ and the corresponding phase ϕ_t are two components of the transmission coefficient [24].

1.1.5 Graphene for performance enhancement

With its exceptional optical properties, graphene, which is made up of a single sheet of carbon atoms arranged in a two-dimensional honeycomb lattice, has the potential to enhance interactions between light and matter[30]. [Graphene Layer] Because of its one-of-a-kind electrical structure as well as its remarkable conductivity, it is an appealing candidate for use in photonics applications. Because graphene can absorb light at frequencies ranging from ultraviolet to terahertz, it can interact with light throughout a wide spectrum of wavelengths. This property of graphene's allows it to be used in a variety of applications. Graphene also has great light confinement and extended interaction lengths, which enables effective light absorption and interaction within a compact footprint. This is made possible by graphene's unique two-dimensional structure. Because of its high carrier mobility, it enables charge delivery that is both quick and efficient, which in turn enables photonic devices to have faster response times. In addition, the fact that graphene's properties may be tuned by electrostatic, chemical, or optical techniques enables dynamic control of its optical qualities, which in turn makes graphene adaptable for use in a wide variety of device topologies. Because graphene possesses these characteristics, it is a good option for improving light-matter interactions in photonic devices, such as tiny ring resonators. This would result in enhanced sensitivity, modulation, and light

manipulation capabilities [31]. This would result in enhanced sensitivity, modulation, and light manipulation capabilities. [Mobility Graphene]

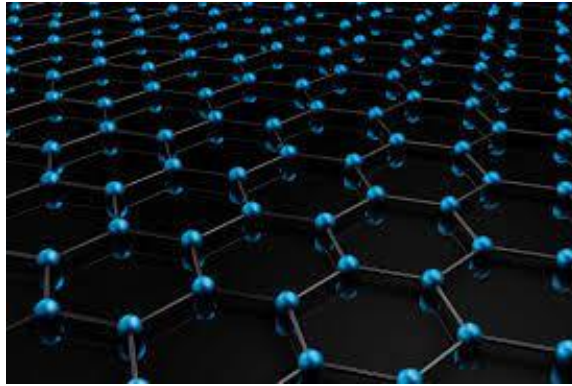


Figure 1.4: Graphene

1.1.6 Gold for performance enhancement

Due to its distinctive optical characteristics, including strong surface plasmon resonance (SPR) and a high extinction coefficient, gold is frequently utilized in photonics devices. Due to these characteristics, gold is the perfect material to increase the sensitivity of optical sensors, such as ring resonator biosensors. For the bulk and affinity sensing of biomolecules, a highly sensitive and miniature hybrid plasmonic ring resonator based on silicon-on-insulator (SOI) technology has been presented. The ring resonator biosensor's improved design prioritizes field enhancement in the narrow slot region to further increase sensitivity. Biomolecules are immobilized on the surface of the gold layer employing the proper surface chemistry. Effective binding is made possible by the positive interaction between the biomolecules and the gold. The hybrid plasmonic waveguide's benefits are also made use of in the optimized design to confine the electric field to the small lower refractive index slot region. The suggested ring resonator biosensor architecture shows the promise for efficient and compact very sensitive affinity sensing [32].

1.1.7 Finite-Difference Time-Domain (FDTD)

A computing approach known as finite-difference time-domain, or FDTD for short, is utilized extensively in the process of solving Maxwell's equations to mimic the behavior of light and how it interacts with matter. It does this by first discretizing space and then time into a grid, after which it calculates the electric and magnetic fields at each individual point in the grid. By numerically solving these equations, FDTD makes it possible to forecast how light travels through different materials and structures, how it reflects, how it refracts, and how it interacts with those materials and structures. When it comes to examining the behavior of photons as they interact with nanostructures, waveguides, and resonators, FDTD simulations are an extremely useful tool in the context of light-matter interaction. It sheds light on the characteristics of electromagnetic fields, including their transmission and reflection coefficients, scattering patterns, and absorption levels. The design and performance of photonic devices, such as micro ring resonators, may be optimized with the use of FDTD simulations by fine-tuning the geometries and materials involved to obtain the required light-matter interaction effects and enhance device efficiency.

The method starts with two of the Maxwell's equations,

$$D \frac{\partial \mathbf{H}}{\partial t} = -\frac{1}{\mu} \nabla \times \mathbf{E}, \quad (1.7)$$

$$D \frac{\partial \mathbf{E}}{\partial t} = \frac{1}{\epsilon} \nabla \times \mathbf{H} \quad (1.8)$$

The electric and magnetic fields are three dimensional vectors. Each equation can be converted into three coupled scalar first order differential equations. The derivatives are both in space and time. The curl operations of equations (1.7) and equation (1.8) yields the following six equations in Cartesian coordinates,

$$\frac{\partial E_z}{\partial y} - \frac{\partial E_y}{\partial z} = \mu \frac{\partial H_x}{\partial t} \quad (1.9)$$

$$\frac{\partial E_x}{\partial z} - \frac{\partial E_z}{\partial x} = \mu \frac{\partial H_y}{\partial t} \quad (1.10)$$

$$\frac{\partial E_y}{\partial x} - \frac{\partial E_x}{\partial y} = \mu \frac{\partial H_z}{\partial t} \quad (1.11)$$

$$\frac{\partial H_z}{\partial y} - \frac{\partial H_y}{\partial z} = \epsilon \frac{\partial E_x}{\partial t} \quad (1.12)$$

$$\frac{\partial H_x}{\partial z} - \frac{\partial H_z}{\partial x} = \epsilon \frac{\partial E_y}{\partial t} \quad (1.13)$$

$$\frac{\partial H_y}{\partial x} - \frac{\partial H_x}{\partial y} = \epsilon \frac{\partial E_z}{\partial t} \quad (1.14)$$

Then the scalar differential equations are transformed into different equations. To achieve that, discretization is needed for both space and time. Yee visualized the field components being arranged within a unit cell for space discretization. Those unit cell edges store electric field components, while magnetic field components are stored in centers. The field components are arranged in such a way where H components are surrounded by four E components and vice versa, which leads to a spatially coupled system of field circulations corresponding to the law of Faraday and Ampere. Fig 1.5 shows the Yee's spatial grid.

Considering a two-dimensional TM (Transverse Magnetic) polarized field case,

$$\frac{\partial E_x}{\partial t} = \frac{1}{\epsilon} \frac{\partial H_y}{\partial y} \quad (1.15)$$

$$\frac{\partial E_x}{\partial t} = \frac{1}{\epsilon} \frac{\partial H_y}{\partial x} \quad (1.16)$$

$$\frac{\partial H_z}{\partial t} = \frac{1}{\mu} \left(\frac{\partial E_y}{\partial y} - \frac{\partial E_x}{\partial x} \right) \quad (1.17)$$

Central difference approximation is applied in each of the equations (1.15), (1.16) and (1.17) which finally conclude in a spatial scalar difference equation in (1.18), (1.19) and (1.20),

$$\frac{\partial E_x}{\partial t} = \frac{1}{\epsilon} \frac{H_z(i,j) - H_z(i,j-1)}{\Delta y} \quad (1.18)$$

$$\frac{\partial E_y}{\partial t} = \frac{1}{\epsilon} \frac{H_z(i,j) - H_z(i-1,j)}{\Delta x} \quad (1.19)$$

$$\frac{\partial H_z}{\partial t} = \frac{1}{\mu} \left(\frac{E_x(i,j+1) - E_x(i,j)}{\Delta y} - \frac{E_y(i+1,j) - E_y(i-1,j)}{\Delta x} \right) \quad (1.20)$$

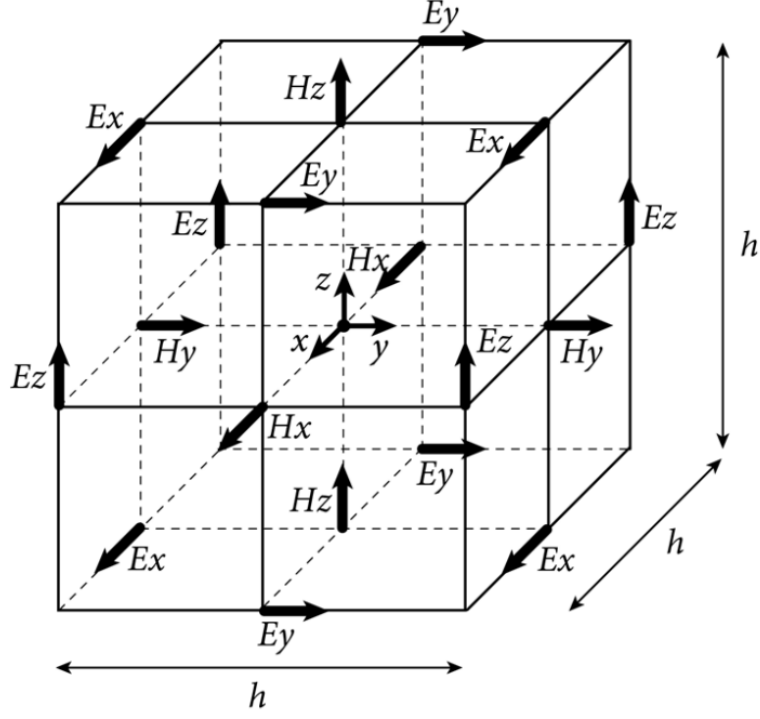


Figure 1.5: Yee's Spatial Grid

To consider the time derivatives, the time axis is to be considered as shown in the figures. The Electric and Magnetic fields are mapped half a step apart along the time axis. Again, applying the central difference approximation the equations (1.18), (1.19) and (1.20) become,

$$\frac{E_x^{n+1}(i+\frac{1}{2},j)-E_x^n(i+\frac{1}{2},j)}{\Delta t} = \frac{1}{\epsilon} \frac{H_x^{n+\frac{1}{2}}(i+\frac{1}{2},j)-H_x^{n+\frac{1}{2}}(i+\frac{1}{2},j-\frac{1}{2})}{\Delta y}, \quad (1.21)$$

$$\frac{E_y^{n+1}(i,j+\frac{1}{2})-E_y^n(i,j+\frac{1}{2})}{\Delta t} = -\frac{1}{\epsilon} \frac{H_z^{n+\frac{1}{2}}(i+\frac{1}{2},j+\frac{1}{2})-H_z^{n+\frac{1}{2}}(i-\frac{1}{2},j+\frac{1}{2})}{\Delta y}, \quad (1.22)$$

$$\frac{H_z^{n+\frac{1}{2}}(i+\frac{1}{2},j+\frac{1}{2})-H_z^{n-\frac{1}{2}}(i+\frac{1}{2},j+\frac{1}{2})}{\Delta t} = -\frac{1}{\mu} \left(\frac{E_x^{n+1}(i+\frac{1}{2},j+1)-E_x^n(i-\frac{1}{2},j)}{\Delta y} - \frac{E_y^n(i,j+\frac{1}{2})-E_y^n(i,j+\frac{3}{2})}{\Delta x} \right), \quad (1.23)$$

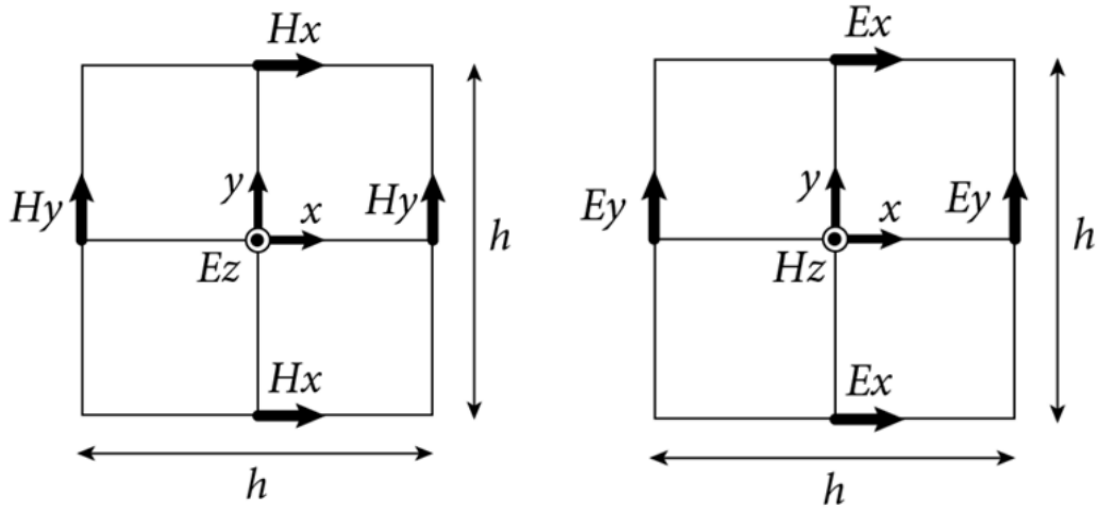


Figure 1.6: Yee's grid in 2D plane

Further simplification of Yee's grid for one dimension gives us,

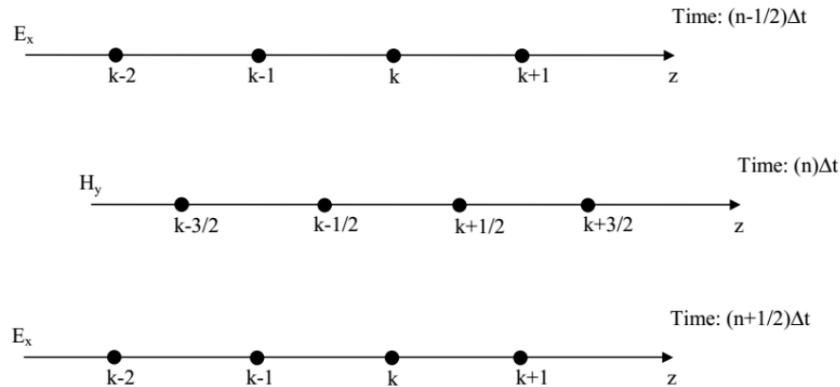


Figure 1.7: Yee's grid in one dimension.

Each field component depends on the field of previous time step itself and the surrounding component in Yee's algorithm. For accurate results, the Yee grid must be 22 numerically stable. In an unstable algorithm the computed magnitude of electric and magnetic field components will gradually increases, making the system unstable. The EM field's propagation should not be faster than the allowed limit imposed by the phase velocity within the material to insure numerical stability. This is done by limiting time step Δt using the Courant-Friedrich-Lewy criterion for the general Yee FDTD grid as follows,

$$\Delta t \leq \left\{ \frac{1}{v_p \sqrt{\frac{1}{(\Delta x)^2} + \frac{1}{(\Delta y)^2} + \frac{1}{(\Delta z)^2}}} \right\}, \quad (1.24)$$

where, Δx , Δy and Δz indicates the spatial Cartesian grid increments.

1.2 Literature Review

Due to their small size, high sensitivity, and compatibility with complementary metal-oxide-semiconductor (CMOS) technology, Silicon-on-Insulator (SOI) Micro Ring Resonators (MRRs) have attracted a lot of interest in the field of photonics and integrated optics. To improve the functionality of SOI MRRs, researchers have investigated various design approaches. The sensitivity and quality factor of the resonators have been improved using strategies including adjusting the ring radius, waveguide width, and coupling techniques. Additionally, to achieve precise control over the device dimensions and lower optical losses, cutting-edge fabrication techniques like reactive ion etching, electron beam lithography, and surface passivation have been used.

SOI MRRs have found applications in a wide range of sensing fields. In biosensing, they enable label-free detection of biomolecules by leveraging the interaction between the target analyte and the evanescent field of the resonator. The sensitivity and specificity of SOI MRR biosensors have been improved through functionalization techniques, such as surface functionalization with specific capture molecules or the integration of additional layers to enhance the interaction with the analyte. Additionally, SOI MRRs have been used for chemical and environmental sensing, demonstrating their potential in detecting gas concentrations, refractive index changes, and pollutant monitoring [33]. [Label free]

Integration of SOI MRRs with other photonic components has been explored to create more complex and multifunctional devices. Integration with Mach-Zehnder interferometers, photodetectors, and heaters has been investigated to enable on-chip sensing systems with enhanced functionality [34]. Moreover, the hybridization of SOI MRRs with other materials, such as polymers or plasmonic structures, has been explored to improve sensitivity, tuneability, or enable specific sensing modalities.

Researchers have focused on developing advanced signal processing techniques to improve the sensitivity and accuracy of SOI MRR-based sensors. Approaches like wavelength interrogation, intensity monitoring, and phase detection have been investigated to extract more precise information from the resonator's output signal. Furthermore, innovative sensing strategies, such as active feedback control, resonance splitting, and Vernier effect-based sensing, have been proposed to enhance the performance of SOI MRR sensors [35].

Despite the significant progress in SOI MRR technology, several challenges remain. The reduction of fabrication costs, integration with CMOS technology, and addressing issues related to temperature stability and drift are areas of ongoing research. Additionally, increasing the sensitivity, miniaturization, and multiplexing capabilities of SOI MRR sensors are areas of active investigation.

In conclusion, SOI MRRs have demonstrated great potential as compact and high-performance devices for various sensing applications. Through continuous advancements in design, fabrication techniques, integration strategies, and signal processing, researchers are making significant strides in enhancing the sensitivity, selectivity, and functionality of SOI MRR-based sensors, paving the way for their integration into practical sensing systems in the future.

1.3 Thesis Objective

Ultimately, our goal is to provide a unique design for a plasmonic refractive index sensor that makes use of a silicon-on-insulator (SOI) micro-ring resonator (MRR) in this body of work. Incorporating an extra layer of graphene and a gold nano disk into the design that has been described here is done with the intention of improving the performance characteristics of the sensor.

We evaluated the performance of the proposed design using the Finite-Difference Time-Domain (FDTD) methodology, a well-known computational method for modeling the interactions of electromagnetic waves. Using FDTD simulations, we were able to gauge the sensor's sensitivity and figure of merit (FOM). These key performance indicators show how well the sensor can pick up changes in the refractive index of the substance around it.

Because of the exceptional optical features that graphene possesses, such as a powerful surface plasmon resonance (SPR) and a high extinction coefficient, the incorporation of a graphene layer

into the design provides several major benefits. Because of the way that this layer interacts with light and the material, the sensor's sensitivity and overall performance are both increased as a direct result.

Furthermore, the integration of a gold nano disk at the heart of the MRR structure takes use of the plasmonic effect, which enables greater light-matter interactions and further increases the sensor's sensitivity. Measurements of the refractive index may be made more sensitively and accurately if graphene and gold nano disks are used together. This combination has a lot of potential.

The concept that has been suggested can be utilized in a variety of contexts, including but not limited to the fields of medical diagnostics, environmental monitoring, and food safety. This plasmonic refractive index sensor can contribute to developments in these domains by reliably detecting changes in the refractive index. This enables precise and real-time monitoring of biological samples, environmental toxins, and food quality, all of which are important for the progress of these fields.

We plan to show the capabilities of this plasmonic refractive index sensor and build the framework for its eventual application in the real world by simulating and evaluating the suggested design using the FDTD approach. This will be done to accomplish both goals. The findings of this study lay the groundwork for future research and development in the field of optical sensing. These discoveries also offer up new opportunities for improving sensor performance and broadening its applications in a variety of different fields of business.

CHAPTER 2

Mechanism of Resonance in Micro ring Resonators And Parameters Analyzed

The performance metrics are indicators of a structure's performance. This section defines two quality parameters for measuring the performance of Micro ring Resonators that are to be used as RI sensors (e.g., Sensitivity, FOM). For all RI sensors, careful optimization of these parameters is critical. In the following sections, advancements in these features are carefully considered for sensing purposes.

2.1 Mechanism of Resonance in Micro Ring Resonators

The resonance concept of a Micro Ring Resonator (MRR) as an optical sensor is based on the phenomena of resonant wavelength changes, which is also discussed in Section 1.4.1 regarding MRRs. The MRR is a small, ring-shaped waveguide structure that is frequently composed of silicon (Si) or other substances having a high refractive index contrast.

The idea of the constructive and destructive interference of light waves can be used to understand the resonance principle. When light enters the MRR, it propagates in the form of a guided mode around the ring's perimeter. A resonant optical mode is created when the light waves continuously recirculate inside the ring.

A particular wavelength at which constructive interference takes place in the MRR's resonant mode causes a high intensity of light to circulate inside the ring. The resonant wavelength or resonant peak is this wavelength.

Any alteration in the surrounding medium's refractive index will have an impact on the guided mode's effective refractive index when the MRR is in contact with an external medium, such as a liquid or gas sample. The MRR's resonant wavelength shifts as a result.

The operating circumstances and design specifications of the MRR determine the typical nonlinear relationship between the shift in the resonant wavelength (λ) and the change in refractive index (n). However, in general, a redshift (longer wavelength) in the resonant peak results from an increase in the external medium's refractive index, whereas a blueshift (shorter wavelength) results from a decrease in refractive index.

The MRR can be used as a sensitive optical sensor for detecting changes in the refractive index of the surrounding medium by measuring the shift in the resonant wavelength. This makes a variety of sensing applications possible, such as chemical analysis, label-free biosensing, measurements of refractive indices, and environmental monitoring.

2.2 Sensitivity

When assessing a micro ring resonator's performance for sensing applications, it's critical to take into account its sensitivity as a refractive index (RI) sensor. Sensitivity in the context of RI sensing refers to the capacity of the micro ring resonator to identify and measure variations in the refractive index of the surrounding medium.

Micro ring resonators are optical components that work on the resonant wavelength shift principle. The resonant wavelength shifts when the refractive index of the medium surrounding the ring resonator changes because it affects the effective refractive index of the guided mode propagating through the ring. This wavelength shift can be used to gauge how sensitive the micro ring resonator is to variations in the local refractive index.

In order to measure the sensitivity of a micro ring resonator as a RI sensor, the change in resonant wavelength per unit change in refractive index, generally abbreviated as $\Delta\lambda/\Delta n$, is typically used. The ability of the micro ring resonator to detect smaller changes in refractive index is shown by a greater sensitivity value.

The design parameters of the ring, like the radius, waveguide width, and coupling regime, can have an impact on the sensitivity of a micro ring resonator as a RI sensor. In general, sensitivity can be improved by decreasing the ring radius and widening the waveguide. Additionally, by lengthening the interaction between the light and the analyte, adjusting the coupling regime (such as under coupling or critical coupling) can maximize the sensitivity.

It is important to keep in mind that a micro ring resonator's sensitivity can also be affected by the resonator's quality factor (Q-factor). Inversely correlated to linewidth, the Q-factor denotes the sharpness of the resonant peak. Better resolution and hence higher sensitivity are made possible by a higher Q-factor.

While sensitivity is a crucial metric for evaluating the performance of a sensor or model, there are certain limitations and challenges that should be considered:

1. **Noise and Interference:** Sensors can be susceptible to various sources of noise and interference, such as environmental fluctuations, electrical noise, or cross-talk from neighboring components. These factors can introduce uncertainties and affect the accuracy and reliability of sensitivity measurements.
2. **Noise and Interference:** Sensors can be susceptible to various sources of noise and interference, such as environmental fluctuations, electrical noise, or crosstalk from neighboring components. These factors can introduce uncertainties and affect the accuracy and reliability of sensitivity measurements.
3. **Detection Limit:** Sensitivity is often limited by the detection limit of the measurement setup or the inherent noise floor of the system. There is a threshold below which small changes in the input signal cannot be reliably detected. Improving the detection limit requires advanced signal processing techniques and noise reduction strategies.
4. **Nonlinear Response:** Some sensors may exhibit nonlinear response characteristics, where the relationship between the input signal and the output response is not linear. This nonlinearity can affect the sensitivity at different operating ranges or introduce complexities in calibration and interpretation of the results.
5. **Cross-Sensitivity:** Sensors designed to measure one specific parameter may exhibit cross-sensitivity to other factors or variables. For instance, an RI sensor may also respond to temperature changes or pressure variations, leading to potential interference or false readings. Understanding and mitigating cross-sensitivity is essential for accurate and selective measurements.
6. **Drift and Stability:** Over time, sensors may experience drift or instability in their response, resulting in a gradual shift in sensitivity. This can be due to aging, environmental effects, or changes in the sensor's characteristics. Maintaining calibration

and monitoring stability are necessary to ensure the reliability of sensitivity measurements.

7. **Sample Preparation and Compatibility:** In certain applications, the sensitivity of a sensor can be affected by the sample preparation process or the compatibility of the sensor with specific analytes or environments. It is crucial to consider these factors and optimize the sensor's design and materials accordingly.
8. **Cost and Scalability:** Developing highly sensitive sensors often involves complex fabrication processes, advanced materials, or sophisticated measurement setups, which can increase the cost and limit scalability. Finding a balance between sensitivity, cost-effectiveness, and manufacturability is a practical challenge [36].

2.3 Figure of Merit (FOM)

The Figure of Merit (FOM) is a statistic that incorporates different performance indicators to assess a sensor's general efficacy and efficiency. The FOM is a crucial metric to evaluate the sensitivity of a micro ring resonator used as a RI sensor in relation to other performance traits. The sensitivity and the quality factor (Q-factor) of the resonator are commonly included in the FOM for a RI sensor based on a tiny ring resonator. Inversely correlated to linewidth, the Q-factor denotes the sharpness of the resonant peak. greater sensitivity is indicated by a greater Q-factor, which also denotes reduced energy loss and better resolution.

The formula for the FOM of a micro ring resonator-based RI sensor is $FOM = Q\text{-factor} / \text{sensitivity}$, where Q-factor denotes the resonator's quality factor and sensitivity the sensitivity measured in terms of wavelength shift per unit change in refractive index.

A sensor with a higher FOM value performs better in terms of sensitivity and resolution. It means that the micro ring resonator can precisely identify even more subtle variations in the refractive index.

It is crucial to give particular information regarding the Q-factor and sensitivity values, as well as the processes applied to their calculation, while describing the FOM of a micro ring resonator in your article. To demonstrate your tiny ring resonator sensor's superior performance, you may also contrast its FOM with those of other existing sensors or methods.

The FOM is a broad metric, thus its applicability will rely on the particular needs and limitations of your application. This is crucial to keep in mind. Therefore, when assessing the overall feasibility of the micro ring resonator as a RI sensor, it is necessary to take into account other pertinent criteria such fabrication complexity, cost, scalability, and compatibility with the target analytes or environment [37].

CHAPTER 3

Main Work

3.1 Recreating and Analyzing Past Models

In this part, we offer our replication of several micro ring resonator (MRR) models by basing them on the most recent work that has been done in the area. The performance of a variety of MRR designs was published in the literature, and it was our goal to reproduce and confirm that performance. To guarantee the accuracy of the replica, we conducted in-depth research on the suggested models, analyzing their geometries and materials.

We reconstructed the MRR structures in simulation software by making use of the information that was presented in the first study. Additionally, we carried out a comprehensive numerical analysis. In each MRR model, we looked at the transmission properties, resonance wavelengths, sensitivity and FOM ranges. The purpose of this exercise was to assess the correctness and dependability of the proposed designs by comparing the outcomes of our simulations with the data that was supplied.

In addition, we investigated the effect that a variety of factors, including the width of the waveguide, the refractive index, and the radius of the ring, had on the performance of the MRRs. We were able to get invaluable insights into the sensitivity and tunability of the resonators by systematically adjusting these parameters in a variety of ways. Because we were able to recreate the MRR models, we were able to evaluate their practicability, robustness, and potential for use in real-world settings.

In general, the results of our recreations of several MRR models offered a full evaluation of the performance characteristics of those models, therefore validating the conclusions that were presented in the original study. We contribute to the knowledge of MRRs and create the groundwork for further research and development in this subject by recreating and assessing these models. This allowed us to go on with our work in this area. Our fundamental ring resonator structure and its parameters prior to optimization are illustrated below. Table 1 exhibits

the geometrical characteristics of the SOI MRR prior to optimization. The ring resonator structure consists of a single waveguide and a micro ring coupled with each other on top of a silicon dioxide substrate as shown in Figure X. The MRR and the straight rectangular waveguide are composed of silicon, whereas the substrate is composed of SiO₂. The width of the rectangular waveguide is denoted by W_1 , and the width of the ring resonator is denoted by W_2 . The distance between the straight waveguide and the MRR is denoted by G , while the total height of the structure is denoted by H .

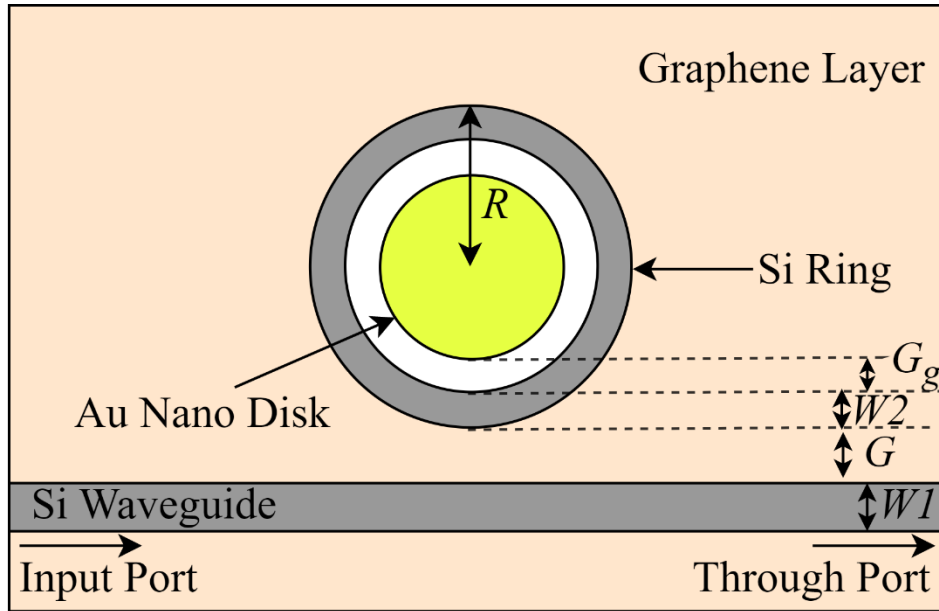


Figure 3.1: Generalized Parameters of SOI MRR

Parameter	Representation	Value	Unit
Height	H	216	nm
Ring Radius	R	3100	nm
Ring width	W_2	400	nm
Gap between waveguide and ring	G	100	nm
Waveguide width	W_1	400	nm

Table 3.1: Geometric parameters of unoptimized MRR.

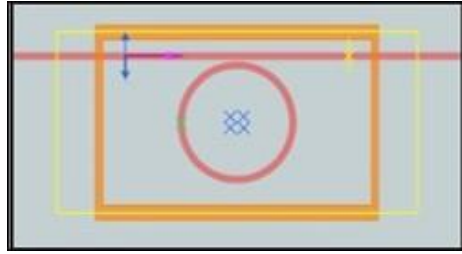


Figure 3.2: Unoptimized SOI MRR Simulation

3.2 Basis of Optimization

One of the most important and often used aspects of the SOI MRR is its ability to detect changes in the refractive index of the dielectric material. Sensitivity (S) and FOM, two metrics that come from the SOI MRR's refractive index sensing capabilities, are crucial for using these devices as sensors.

The sensitivity is affected by the shift in the resonant wavelength peak caused by the material's altered refractive index. Equation can be used to compute it [14].

$$S = \frac{d\lambda}{dn}$$

On the other hand, the resonance spectrum's sensitivity, and Full Width Half Maxima (FWHM) can be used to compute FOM. To express FOM, we use the equation[14],

$$FOM = \frac{S}{FWHM}$$

For the purposes of optimization analysis, the parameter values listed in Table 1 are regarded as the base values. The analysis's refractive index ranged from 1.348 to 1.351. The FDTD approach is used to conduct a numerical analysis in accordance with the transmission spectrum. Every analysis is done for the source's fundamental mode at the input port, and the resonant wavelength changes linearly as the refractive index changes.

3.3 Optimization of Geometric Dimensions of MRR

Our next work was to investigate methods for improving the performance of the micro ring resonator (MRR) structure by adjusting the geometric dimensions of its components. We did not

use optimization algorithms; rather, we manually modified these dimensions by defined increments and then ran further simulations to analyze the changes in sensitivity and Figure of Merit (FOM) that resulted from these adjustments.

We conducted a systematic investigation into the relationships between the device's performance and its geometric characteristics, such as the ring radius, ring width, waveguide width, gap between the ring and waveguide, and MRR structure height. This investigation was carried out by gradually shifting the device's geometric dimensions. After making each modification, we re-stimulated the MRR and analyzed its response. We concentrated on the sensitivity, which indicates the device's capacity to detect changes in the refractive index of the surrounding medium, and the FOM, which combines sensitivity and linewidth to measure overall performance.

Using this method for manually optimizing the system, we were able to determine the dimensions that led to the maximum sensitivity and FOM values. We got insights into how changes in the geometric dimensions impacted the behavior of the MRR by first examining the simulation results and then noting the trends that emerged from those simulations. Because of this knowledge, we were able to draw educated conclusions regarding the best dimensions that would lead to an improvement in performance.

In general, our manual modification and simulation technique was successful in providing useful insights into the effect that geometric dimensions have on the sensitivity and FOM of the MRR. These findings provided more insight into the design process and highlighted the relevance of picking dimensions that are appropriate for the MRR device in question to achieve optimal performance.

3.3.1 Optimization of the Rectangular Waveguide Width (W_1)

The rectangular waveguide, W_1 , has a width that ranges from 350 nm to 500 nm. Keeping all other variables fixed as given in Table 1 and using 4 different values, the transmission spectrum is displayed in Figure 3.4 (a). The resonant wavelengths are where the dip appears. When W_1 is increased, the values of sensitivity and FOM rise consistently, peaking at 400 nm, then falling to eventually achieve constant values. Therefore, 400nm was chosen as the width of our optimal structure. Figures 3.4 (b) and (c) show the fluctuation of these performance characteristics,

respectively. Figure 3.4 (d) shows that red shift increases as the rectangular waveguide's width is increased.

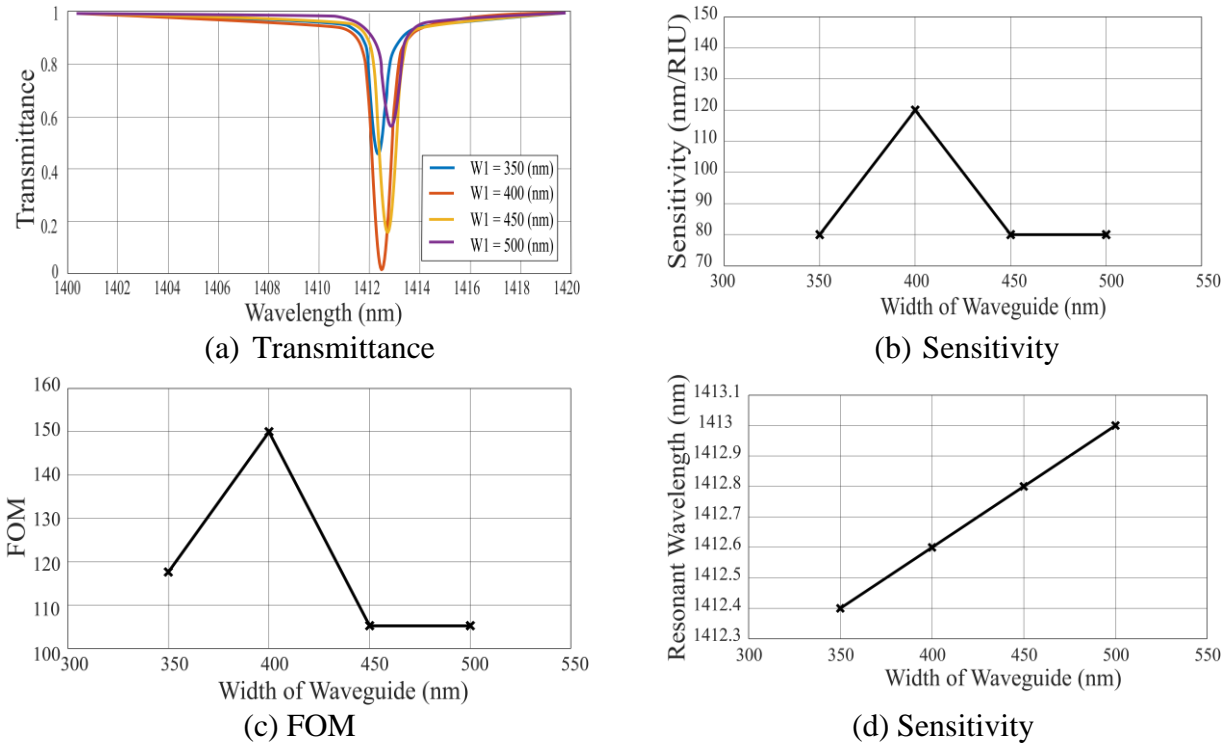


Figure 3.3: (a) Transmission characteristics and (b), (c), (d) change in performance parameter with change in Width of rectangular waveguide, W_1

3.3.2 Optimization of the Resonator Height (H)

With a step size of 1 nm, the height H of the ring and rectangular waveguide ranges from 216 nm to 219 nm. All other parameters remained constant while testing for this one. Transmittance is shown on the vertical axis in Figure 3.5(a), while wavelength is shown on the horizontal axis. Figures 3.5(b) and 3.5(c) illustrate how changing H affects sensitivity and FOM. When we increase the height, we observe a red shift, as shown in Figure 3.5(d). Sensitivity and FOM diminish linearly as H is raised from 216 to 217 nm. After 217 nm, both sensitivity and FOM consistently increase before declining once more after 218 nm. As a result, we were able to achieve the highest sensitivity and FOM for our optimized structure at a height of 218 nm.

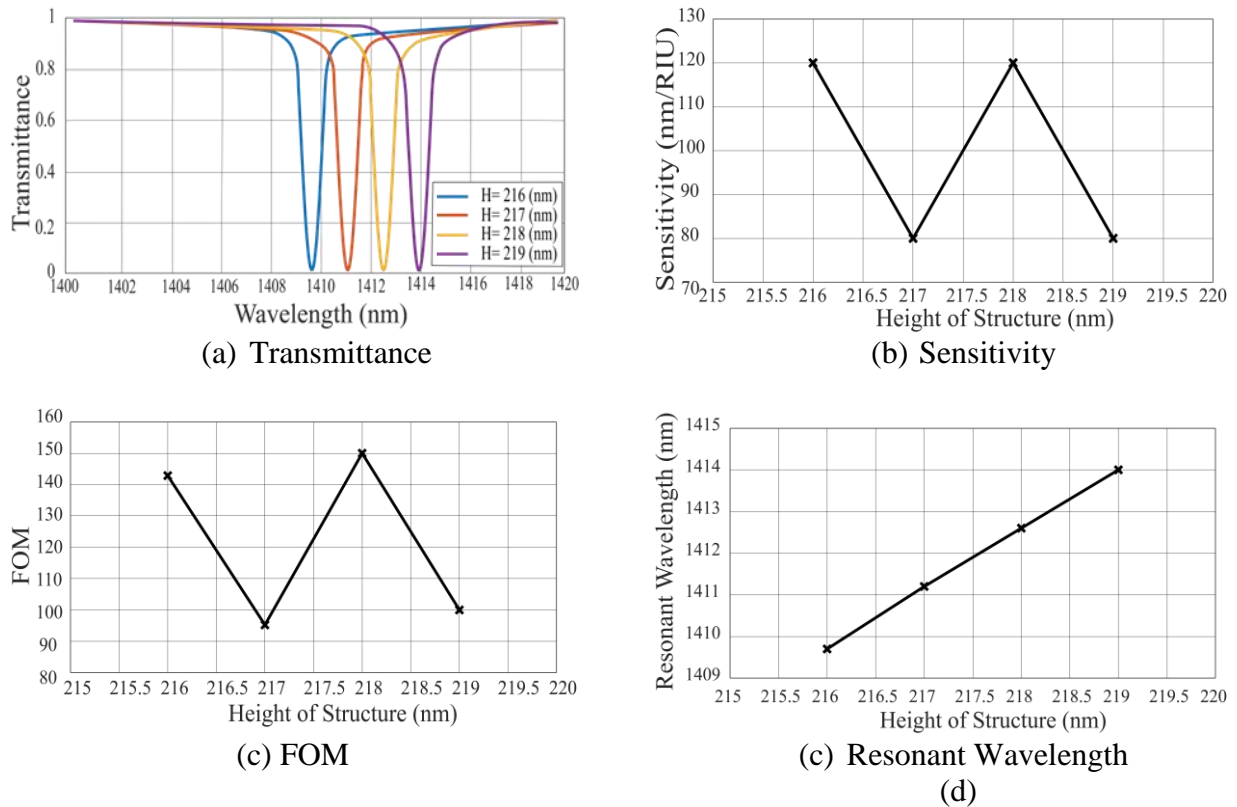


Figure 3.4: (a) Transmission characteristics and (b), (c), (d) change in performance parameter with change in Height, H

3.3.3 Optimization of the Coupling Gap (G)

Figure 3.6 (a) displays the transmittance as a function of wavelength while maintaining consistency across all parameters and adjusting the coupling gap G between the ring and rectangular waveguide from 40 nm to 100 nm. The variations in sensitivity and FOM are seen in Figures 3.6 (b) and 3.6(c), respectively. It was found that the performance characteristics altered erratically as the coupling gap grew. The sensitivity alternately dropped and increased, and the FOM trended similarly nonlinearly. The coupling gap of our optimized structure, which is 40 nm, was shown to have the greatest results for both sensitivity and FOM. The shifting resonance peaks are shown in Figure 3.6 (d).

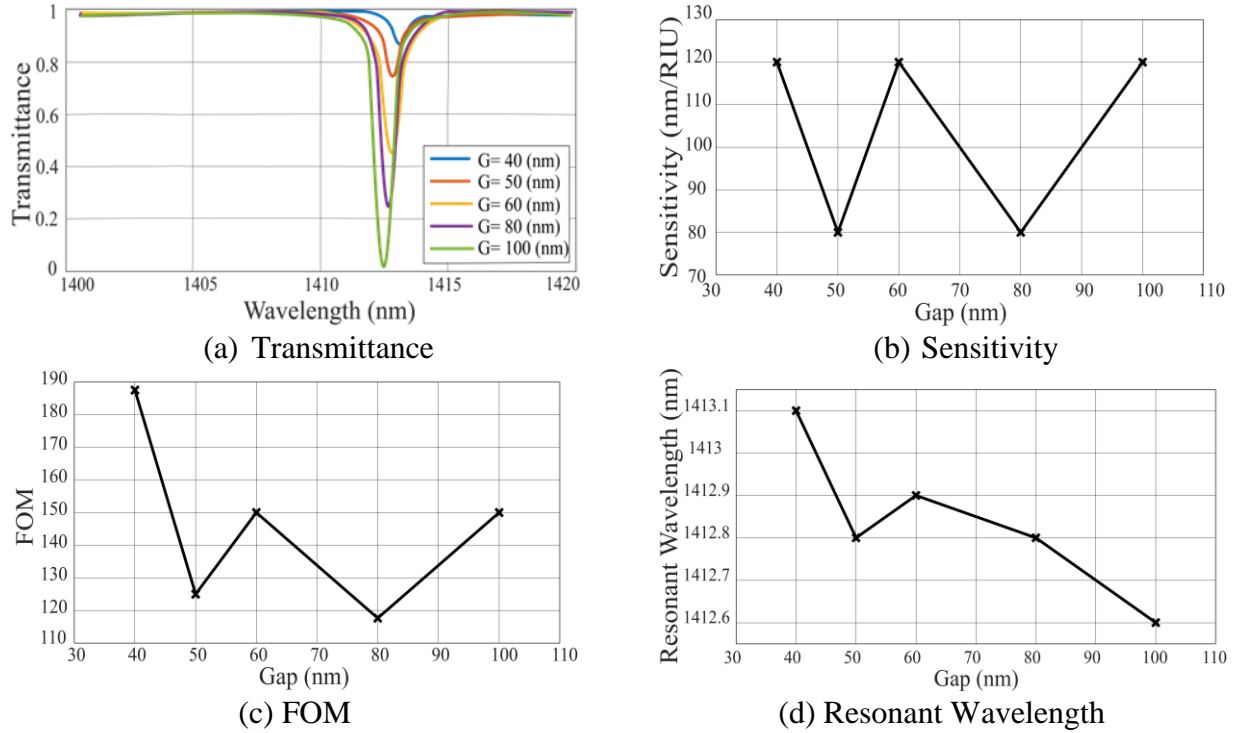
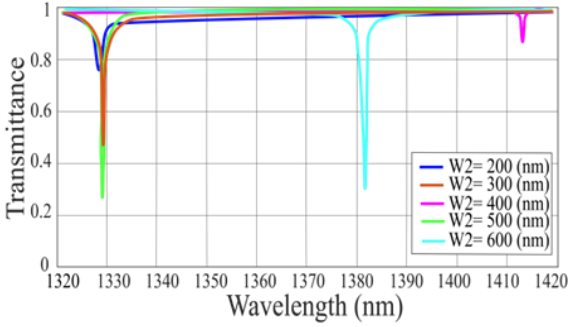


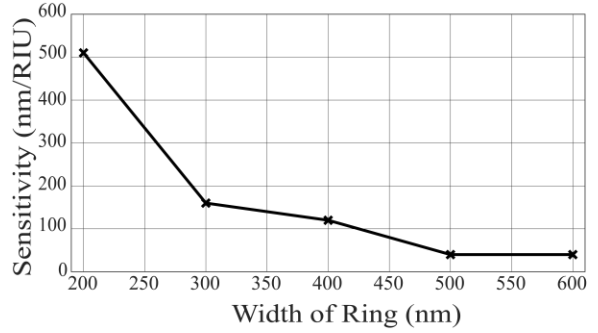
Figure 3.5:(a) Transmission characteristics and (b), (c), (d) change in performance parameter with change in coupling gap, G

3.3.4 Optimization of the Ring Width (W_2)

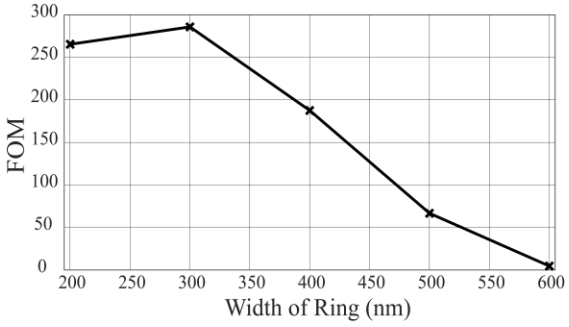
Investigating the width of ring W_2 , transmission spectra are produced for five equally spaced values from 200 nm to 600 nm. Figures 3.7(b) and 3.7(c) show the transmission seen in Figure 3.7(a), together with the performance metrics related to it. The resonant peak changes are well-illustrated in Figure 3.7(d). However, there is a modest rise in FOM from 200 nm to 30 nm. Overall, the sensitivity and FOM decrease as W_2 is increased. The maximum sensitivity was noted at a ring width of 200 nm, paired with an extraordinarily high FOM. As a result, 200nm was chosen as our optimal ring width.



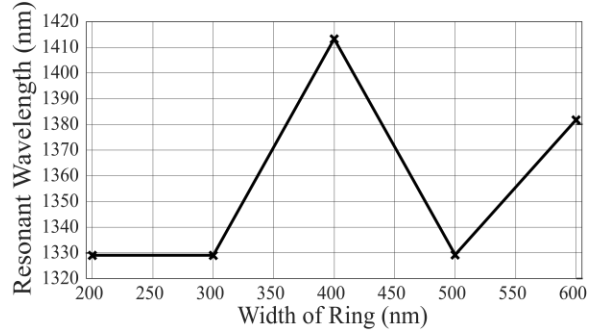
(a) Transmittance



(b) Sensitivity



(c) FOM



(d) Resonant Wavelength

Figure 3.6: (a) Transmission characteristics and (b), (c), (d) change in performance parameter with change in width of ring, W_2

3.3.5 Optimization of the Ring Radius (R)

The transmission characteristic for variations in the ring's radius, R , may be noticed when Figure 3.8 (a) is examined. The measurement ranges from 2100 nm to 5100 nm with a 1000 nm interval. Figures 3.8 (b) and 3.8 (c) show the sensitivity and FOM, respectively. The value of sensitivity rises practically linearly when R is raised. FOM, however, rises to a radius value of 4100 nm before falling. A ring radius of 5100 nm therefore provided the optimal balance between sensitivity and FOM. Figure 3.8 (d) depicts the shift in resonance peak in detail.

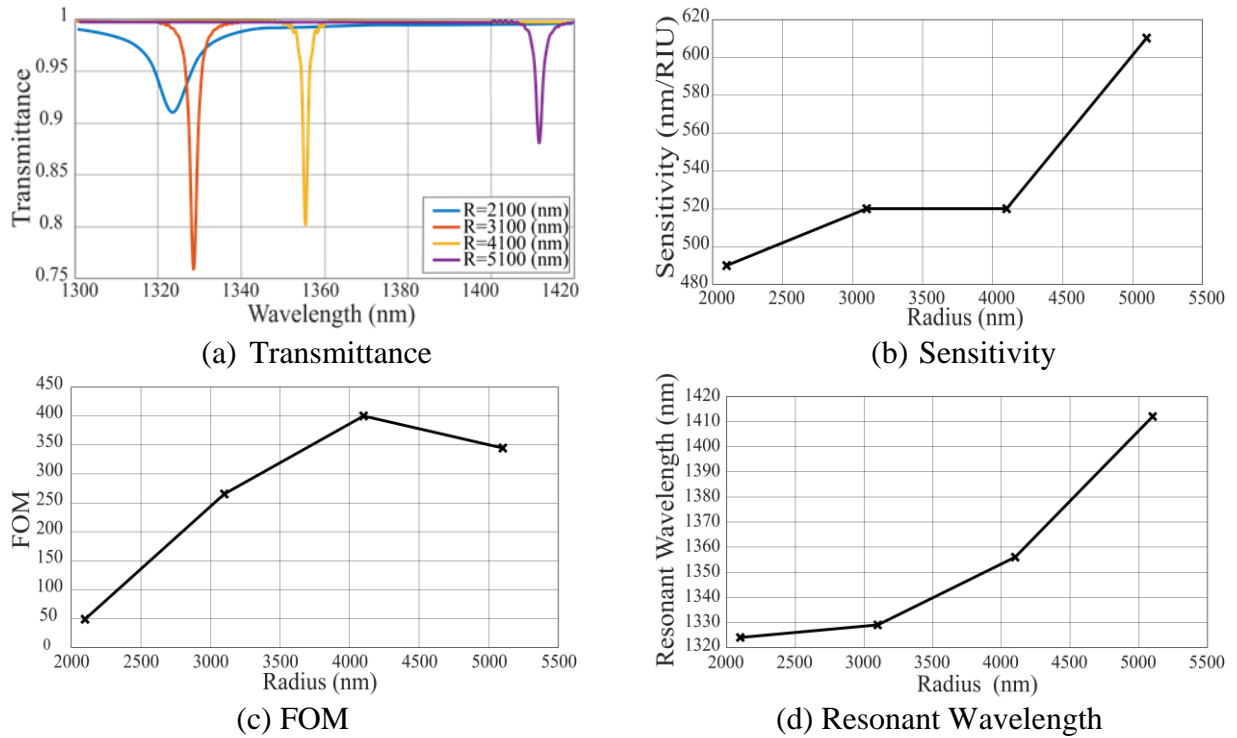


Figure 3.7: (a) Transmission characteristics and (b), (c), (d) change in performance parameter with radius of ring, R

3.3.6 Optimized Simple Ring Resonator

Therefore, after the optimization, the parameters that gave the best performance resulted in a sensitivity of 610 nm/RIU with a corresponding FOM of 344. Both are very high optimized values that is obtained from FDTD analysis of our initial model.

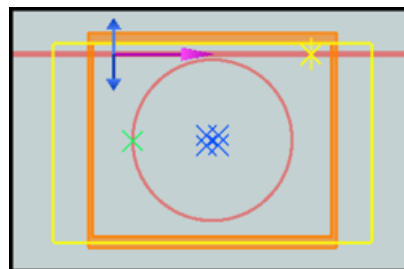


Figure 3.8: Optimized SOI MRR Simulation

3.4 Scope of Improvement

While optimization of the basic Ring Resonator structure increases the sensitivity and the FOM significantly, there are other additions that can be made to the existing optimized structure that can further enhance the performance of the ring resonator. We have mainly focused on two main methods.

3.4.1 Depositing Graphene Layer

When a graphene monolayer was deposited on the model it modifies the effective refractive index due to the presence of the analyte. By adjusting the external electric field and tuning the refractive index of graphene, the evanescent field of the SOI ring resonator may be changed. Furthermore, the improved carrier dynamics of graphene assist the motion of surface plasmons along the graphene surface. These plasmons can drastically alter the evanescent field's properties in the ring resonator by strongly interacting with it [26].

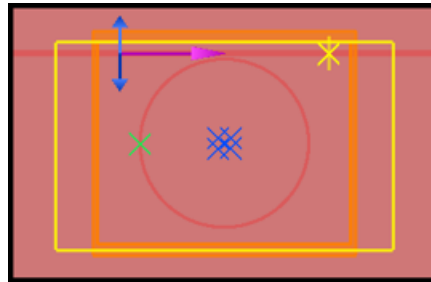


Figure 3.9: Optimized SOI MRR with Graphene Simulation

3.4.2 Adding Gold Nano Disc

To further increase sensitivity, a silicon ring and a gold layer in the form of a disc has been positioned around the silicon dioxide layer. The gold layer and the evanescent field that emerges from the ring can interact powerfully. The localized surface plasmons are excited when the gold disc interacts with the evanescent field region, which significantly increases the electric field

intensity at the gold layer's surface. At resonance, the total electric fields near-gold disc amplitude can dramatically rise above the incident amplitude. High sensitivity values are possible because of the field accumulation in the gap area. The effect of the analyte on the effective refractive index is amplified when gold is added, raising the sensitivity [23].

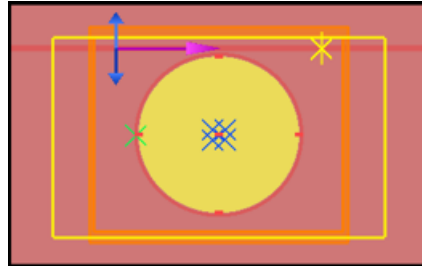


Figure 3.10: Optimized SOI MRR with Gold Simulation

CHAPTER 4

Results and Discussion

The FDTD approach is used to validate the structural simulation. The suggested design's parameters vary until we get optimized values, which give the highest sensitivity and FOM.

4.1 Results

After the optimization process was complete, the settings that offered the highest performance resulted in a sensitivity of 610 nm/RIU with a FOM value that corresponded to 344. Both parameters were tuned to extremely high levels after being run through FDTD and applied to our basic model. Table 2 presents the associated parameters for your perusal. In terms of sensitivity, the results of our improved and optimized refractive index sensor have been superior to those of recent studies. When compared to Kumari et al. [17], which our improved device outperforms, we achieve a significant increase in sensitivity of approximately 10 percent. This is a significant improvement.

Parameter of Optimized Structure	Representation	Value	Unit
Height	H	218	nm
Ring Radius	R	5100	nm
Ring width	W_2	200	nm
Gap between waveguide and ring	G	40	nm
Waveguide width	W_1	400	nm
Gap between gold nano disk and micro-ring	Gg	66	nm

Table 4.2: Optimized Geometric Parameters.

Paper	Year	Sensitivity (nm/RIU)
C . I. Arce et al. [38]	2010	70
Nugroho et al. [39]	2020	85.84
C. Ciminelli et al. [40]	2013	120
M.Grist et al.[27]	2013	142
F. Khozeymeh et al. [25]	2018	193
T. Claes et al. [41]	2009	298
R.Raj et al.[42]	2018	360
S.Kumari et al. [32]	2022	555
Proposed Sensor (This paper)	2023	610

Table 4.3: Comparison of sensitivities with previous publications.

4.2 Performance enhancement after addition of Gold and Graphene

Adding a graphene monolayer to the substrate is the first step that must be taken to further improve the performance of the SOI MRR after it has already been improved. Immediate improvement can be seen in the situation. The FOM has been brought down to 118 while the sensitivity has been raised to 680 nm/RIU. Both fundamental principles. We evaluated the optimized SOI MRR model with a gold disc placed inside the MRR to get a better level of sensitivity. A gap known as Gg is kept between the gold disc and the MRR. The value of the gap is determined to be 66 nm, which is the same amount as Kumari et al. [17] utilized. This results in a sensitivity of 690 nm/RIU and a FOM of 69, respectively. This leads to the formation of a hybrid structure that performs better than any of those shown in Table 3 and further raises the sensitivity of the optimized model to 730 while simultaneously decreasing its FOM to 56.15, which is a value that we are willing to accept. As a result, an improvement in sensitivity of 31.53 percent on average is obtained. At the time of this investigation, this figure represents the highest possible.

CHAPTER 5

Conclusion

5.1 Conclusion

In conclusion, this study presents a simulation-based design for a highly sensitive Silicon-On-Insulator (SOI) ring resonator with a Figure of Merit (FOM) of 56.15 and high sensitivity of 730 nm/RIU. The proposed design incorporates a graphene 2D layer and a gold nano disk to improve the material's response to light and increase sensitivity. The results demonstrate the potential of this device as a high-performance on-chip refractive index nano-sensor. The study also discusses the optimization of the design and the calculation of sensitivity, FOM, and sensing resolution. Additionally, the article provides a list of references for various types of biosensors based on SOI technology, including ring resonators, mirroring resonators, and slot waveguide-based sensors, covering topics such as plasmonic sensors, glucose sensing, label-free biosensing, and hybrid plasmonic-photonic sensors. Overall, this study provides valuable insights into the design and optimization of SOI-based ring resonators for use as refractive index sensors and highlights the potential of these devices for a wide range of biosensing applications.

5.2 Future Work

The suggested architecture can be expanded upon in future work, and the performance metrics of the SOI-based refractive index sensors can be examined. The addition of graphene and gold to the regular optimized MRR structure can pave the way for the creation of more precise and potent sensors for a variety of applications, including chemical and biological detection. The potential of the suggested design for other applications, such as biosensing, environmental monitoring, and medical diagnostics, can be investigated through further research. In order to increase the sensitivity and effectiveness of the sensors, it is also possible to examine the use of different materials and structures. Overall, the research offers a potential method for creating high-performance on-chip refractive index nano-sensors, and future work can concentrate on refining and enhancing the suggested design for various uses.

Future work can be done by building upon the suggested design and analyzing the performance parameters of the SOI-based refractive index sensors. The incorporation of graphene and gold into the structure of a regular optimized MRR can be a steppingstone towards the development of more accurate and effective sensors for various uses, including chemical and biological sensing. Further studies can be conducted to explore the potential of the suggested design for other applications, such as biosensing, environmental monitoring, and medical diagnostics. Additionally, the use of other materials and structures can be investigated to improve the sensitivity and performance of the sensors. Overall, our research and analysis provide a promising approach for the development of high-performance on-chip refractive index nano-sensors, and future work can focus on optimizing and improving the suggested design for various applications.

References

- [1] A. Yacoubian, “Optical Sensing,” *Opt. Essentials*, pp. 107–123, 2018, doi: 10.1201/9781315216324-10.
- [2] F. A. Said, P. S. Menon, S. Shaari, and B. Y. Majlis, “FDTD Analysis on Geometrical Parameters of Bimetallic Localized Surface Plasmon Resonance-Based Sensor,” *Proc. - Int. Conf. Intell. Syst. Model. Simulation, ISMS*, vol. 2015-October, pp. 242–245, 2015, doi: 10.1109/ISMS.2015.12.
- [3] M. R. Rakhshani and M. A. Mansouri-Birjandi, “Engineering Hexagonal Array of Nanoholes for High Sensitivity Biosensor and Application for Human Blood Group Detection,” *IEEE Trans. Nanotechnol.*, vol. 17, no. 3, pp. 475–481, 2018, doi: 10.1109/TNANO.2018.2811800.
- [4] J. Dong *et al.*, “Compact notch microwave photonic filters using on-chip integrated microring resonators,” *IEEE Photonics J.*, vol. 5, no. 2, pp. 0–7, 2013, doi: 10.1109/JPHOT.2013.2245883.
- [5] M. B. Wabuye and T. Vo-dinh, “Detection of Human Immunodeficiency Virus Type 1 DNA Sequence Using Plasmonics Nanoprobes,” vol. 77, no. 23, pp. 7810–7815, 2008.
- [6] R. Boeck, M. Caverley, L. Chrostowski, and N. A. F. Jaeger, “Experimental demonstration of a silicon-on-insulator high-performance double microring filter using MZI-based coupling,” vol. 40, no. 2, pp. 276–279, 2015.
- [7] P. Dumon, W. Bogaerts, P. De Heyn, T. Van Vaerenbergh, K. De Vos, and S. Kumar, “Silicon microring resonators Silicon microring resonators,” no. February 2014, 2012, doi: 10.1002/lpor.201100017.
- [8] M. Y. Azab, M. F. O. Hameed, A. M. Nasr, and S. S. A. Obayya, “plasmon photonic crystal fiber biosensor,” *Opt. Quantum Electron.*, vol. 50, no. 2, pp. 1–13, 2018, doi: 10.1007/s11082-017-1302-2.
- [9] N. Fabri-faja *et al.*, “AC SC,” *Anal. Chim. Acta*, 2019, doi: 10.1016/j.aca.2019.05.038.

- [10] Y. Ding *et al.*, “Towards Polarization Diversity on the SOI Platform,” vol. 23, no. 23, pp. 1808–1810, 2011.
- [11] Y. Xu *et al.*, “Optical Refractive Index Sensors with Plasmonic and Photonic Structures : Promising and Inconvenient Truth,” vol. 1801433, pp. 31–33, 2019, doi: 10.1002/adom.201801433.
- [12] L. Qiao, G. Zhang, Z. Wang, G. Fan, and Y. Yan, “Study on the fano resonance of coupling M-type cavity based on surface plasmon polaritons,” *Opt. Commun.*, vol. 433, no. June 2018, pp. 144–149, 2019, doi: 10.1016/j.optcom.2018.09.055.
- [13] W. L. Barnes, A. Dereux, and T. W. Ebbesen, “Surface plasmon subwavelength optics,” *Nature*, vol. 424, no. 6950, pp. 824–830, 2003, doi: 10.1038/nature01937.
- [14] R. Al Mahmud, M. O. Faruque, and R. H. Sagor, “A highly sensitive plasmonic refractive index sensor based on triangular resonator,” *Opt. Commun.*, vol. 483, p. 126634, 2021, doi: 10.1016/j.optcom.2020.126634.
- [15] J. Doevenspeck, “Plasmonics : Circuit and system-level evaluation for beyond-CMOS applications,” 2016.
- [16] *No Title.*
- [17] W. Bogaerts, P. Dumon, D. Van Thourhout, and R. Baets, “Low-loss , low-cross-talk crossings for silicon-on-insulator nanophotonic waveguides,” vol. 32, no. 19, pp. 2801–2803, 2007.
- [18] M. Polytec, “Using SOI to Achieve Low-Power Consumption in Digital,” pp. 14–17, 2005.
- [19] C. Chuang, P. Lu, and C. J. Anderson, “SOI for Digital CMOS VLSI : Design Considerations and Advances,” vol. 86, no. 4, pp. 689–720, 1998.
- [20] E. Kasper and J. Yu, “Microring Resonators,” *Silicon-Based Photonics*, vol. 29, no. 24, pp. 49–93, 2020, doi: 10.1201/9781315156514-4.
- [21] P. Colinge, “2 Basics of Silicon-on-Insulator (SOI) Technology,” 2004.
- [22] W. Bogaerts *et al.*, “Fabrication of photonic crystals in silicon-on-insulator using 248-nm

- deep UV lithography,” *IEEE J. Sel. Top. Quantum Electron.*, vol. 8, no. 4, pp. 928–934, 2002, doi: 10.1109/JSTQE.2002.800845.
- [23] A. Bozzola, S. Perotto, and F. De Angelis, “Hybrid plasmonic-photonic whispering gallery mode resonators for sensing: A critical review,” *Analyst*, vol. 142, no. 6, pp. 883–898, 2017, doi: 10.1039/c6an02693a.
- [24] R. Arefin, O. Faruque, R. Al Mahmud, and R. H. Sagor, “Design of a tunable ring resonator with enhanced quality factor,” *Proc. 9th Int. Conf. Electr. Comput. Eng. ICECE 2016*, no. 1, pp. 369–372, 2017, doi: 10.1109/ICECE.2016.7853933.
- [25] F. Khozayemeh and M. Razaghi, “Characteristics optimization in single and dual coupled silicon-on-insulator ring (disk) photonic biosensors,” *Sensors Actuators, B Chem.*, vol. 281, no. October 2018, pp. 998–1008, 2019, doi: 10.1016/j.snb.2018.11.017.
- [26] M. Iqbal *et al.*, “Label-Free Biosensor Arrays Based on Silicon,” *IEEE J. Sel. Top. Quantum Electron.*, vol. 16, no. 3, pp. 654–661, 2010.
- [27] S. M. Grist *et al.*, “Silicon photonic micro-disk resonators for label-free biosensing,” *Opt. Express*, vol. 21, no. 7, p. 7994, 2013, doi: 10.1364/oe.21.007994.
- [28] C. Y. Zhao, P. Y. Chen, P. Y. Li, and C. M. Zhang, “Numerical analysis of effective refractive index bio-sensor based on graphene-embedded slot-based dual-micro-ring resonator,” *Int. J. Mod. Phys. B*, vol. 34, no. 17, 2020, doi: 10.1142/S0217979220501453.
- [29] J. Zhou, W. Wang, Y. Wang, J. Feng, and J. Guo, “A highly-sensitive NaCl concentration sensor based on a compact silicon-on-insulator micro-ring resonator,” *AOPC 2015 Opt. Optoelectron. Sens. Imaging Technol.*, vol. 9674, p. 96742F, 2015, doi: 10.1117/12.2201034.
- [30] G. Photonics and A. S. P. Excitations, “Graphene Photonics, Plasmonics and Optoelectronics,” no. c, 2013.
- [31] F. Bonaccorso, Z. Sun, T. Hasan, and A. C. Ferrari, “Graphene photonics and optoelectronics,” vol. 4, no. August, pp. 611–622, 2010, doi: 10.1038/nphoton.2010.186.
- [32] S. Kumari and S. M. Tripathi, “Hybrid Plasmonic SOI Ring Resonator for Bulk and

- Affinity Bio - sensing Applications,” *Silicon*, vol. 14, no. 17, pp. 11577–11586, 2022, doi: 10.1007/s12633-022-01877-3.
- [33] X. Li *et al.*, “Sensitive label-free and compact biosensor based on concentric silicon-on-insulator microring resonators,” *Appl. Opt.*, vol. 48, no. 25, pp. 3–7, 2009, doi: 10.1364/AO.48.000F90.
- [34] P. Dainesi *et al.*, “CMOS compatible fully integrated Mach-Zehnder interferometer in SOI technology,” *IEEE Photonics Technol. Lett.*, vol. 12, no. 6, pp. 660–662, 2000, doi: 10.1109/68.849076.
- [35] Z. Zhang, M. Dainese, L. Wosinski, and M. Qiu, “<Oe-16-7-4621.Pdf>,” vol. 16, no. 7, pp. 4621–4630, 2008.
- [36] O. Levi *et al.*, “Sensitivity analysis of a photonic crystal structure for index-of-refraction sensing,” *Nanoscale Imaging, Spectrosc. Sensing, Actuation Biomed. Appl. IV*, vol. 6447, p. 64470P, 2007, doi: 10.1117/12.705670.
- [37] H. G. Balian and N. W. Eddy, “Figure-of-merit (FOM), an improved criterion over the normalized chi-squared test for assessing goodness-of-fit of gamma-ray spectral peaks,” *Nucl. Instruments Methods*, vol. 145, no. 2, pp. 389–395, 1977, doi: 10.1016/0029-554X(77)90437-2.
- [38] C. Lerma Arce, K. De Vos, T. Claes, K. Komorowska, D. Van Thourhout, and P. Bienstman, “Silicon-on-insulator microring resonator sensor integrated on an optical fiber facet,” *IEEE Photonics Technol. Lett.*, vol. 23, no. 13, pp. 890–892, 2011, doi: 10.1109/LPT.2011.2143704.
- [39] H. S. Nugroho *et al.*, “Silicon on insulator-based microring resonator and Au nanofilm Krestchmann-based surface plasmon resonance glucose sensors for lab-on-a-chip applications,” *Int. J. Nanotechnol.*, vol. 17, no. 1, pp. 29–41, 2020, doi: 10.1504/IJNT.2020.109348.
- [40] C. Ciminelli, F. Dell’Olio, D. Conteduca, C. M. Campanella, and M. N. Armenise, “High performance SOI microring resonator for biochemical sensing,” *Opt. Laser Technol.*, vol. 59, pp. 60–67, 2014, doi: 10.1016/j.optlastec.2013.12.011.

- [41] T. Claes, J. G. Molera, K. De Vos, E. Schacht, R. Baets, and P. Bienstman, "Label-free biosensing with a slot-waveguide-based ring resonator in silicon on insulator," *IEEE Photonics J.*, vol. 1, no. 3, pp. 197–204, 2009, doi: 10.1109/JPHOT.2009.2031596.
- [42] R. R. Singh, S. Kumari, A. Gautam, and V. Priye, "Glucose Sensing Using Slot Waveguide-Based SOI Ring Resonator," *IEEE J. Sel. Top. Quantum Electron.*, vol. 25, no. 1, pp. 1–8, 2018, doi: 10.1109/JSTQE.2018.2879022.